

Unique Interactions Between Diborane and π Orbitals: Blue- or Red-Shifted Hydrogen Bonding?

Shan Xi Tian,* Hai-Bei Li, Yubin Bai, and Jinlong Yang

Hefei National Laboratory for Physical Sciences at the Microscale and Department of Chemical Physics, University of Science and Technology of China, Hefei, Anhui, 230026, China

Received: April 2, 2008; Revised Manuscript Received: June 22, 2008

A new type of hydrogen-bonding interaction in the diborane (B_2H_6) $\cdots\pi$ (benzene C_6H_6 , 1,3-cyclopentadiene C_5H_6 , and cyclobutadiene C_4H_4) system is identified with the natural bond orbital and atoms-in-molecules analyses based on ab initio calculations. In comparison with the symmetric and asymmetric stretching vibrational modes of the bridging hydrogen atoms in free B_2H_6 , the frequencies of the symmetric mode are red-shifted for $B_2H_6\cdots C_6H_6$ and $B_2H_6\cdots C_5H_6$ but blue-shifted for $B_2H_6\cdots C_4H_4$. The frequency blue shifts of the asymmetric mode are found for all three complexes; the most significant blue shift is 14.73 cm^{-1} for the asymmetric mode in $B_2H_6\cdots C_4H_4$. In these complexes, the electron-deficient three-center two-electron bond $B-H_1-B$ facing the π orbital is shortened, while the opposite $B-H_2-B$ bond is elongated.

1. Introduction

It is well-known that hydrogen bonding (HB) is a broader phenomenon than previously accepted.¹ However, it is not easy to define HB, including all of the features in the different branches of science. Even though an electrostatic origin was historically considered,² it is now clear that depending on the strength of the HBs, other contributions are additionally present.³ According to the classical electrostatic model $X-H\cdots Y$, if the significant charge transfer (CT) occurs from the proton acceptor Y to the proton donor, that is, the lone pair orbital n_Y to the σ_{X-H}^* antibonding orbital, the X–H bond should be weakened upon the HB formation and concomitantly elongated.⁴ This elongation of the X–H bond results in a decrease of the X–H stretching vibration frequency, and such a frequency red shift with respect to that of the free monomer has been used as the fingerprint of HB complexes in many experimental studies.⁵ On the other hand, a few improper HB complexes are found in the experiments. Namely, the X–H stretching vibrational frequency is observed to shift to a higher frequency (i.e., blue-shifted), together with a contraction of the X–H bond, especially including the $X-H\cdots Y$ interactions where X is CF_3 or CCl_3 and Y is triflylmethane, benzene, ethylene oxide, or dimethyl ether.^{6–12} Li et al. found that $F_3SiH\cdots OH_2$, $F_2NH\cdots FH$, $F_2PH\cdots NH_3$, and $F_2PH\cdots OH_2$ also exhibited the substantial blue-shifted HB characteristics.¹³ Therefore, the blue-shifted HBs do not require either a carbon center or the absence of a lone pair on the proton donor.^{12–14} The mechanism of the blue-shifted HB is still inconclusive. Several theoretical approaches are briefly introduced here. One attributes the X–H bond contraction to the short-range Pauli repulsive force.^{13,15} Another one was proposed by Hobza and co-workers, for example, in a complex $ClC-H_3\cdots F-H$; after the CT proceeded from the lone-pair orbital n_F to the remote antibonding orbital σ_{C-Cl}^* , a structural reorganization led to the contraction of the C–H bond lengths.^{11,12,16–18} The electrostatic contributions to the improper HBs were proposed as the electric field effect that the isolated proton donor (e.g., C–H) had a negative derivation of dipole

moment along the stretching coordinates, that is, $d\mu^0/dr < 0$ or C–H bond shortening, as well as the stronger exchange interaction.^{19,20} Recently, two balance models emerged as follows: Alabugin et al. suggested that there was a subtle balance between the hyperconjugative bond weakening and the rehybridization (the latter strengthens the bond by enhancing the percent s-character of the X atom in the X–H bond due to the presence of Y);²¹ the other balance model presented by Joseph and Jemmis is that the electron affinity of X results in a net gain of electron density at the X–H bond region as the coexistence of Y, hereby leading to the X–H bond contraction, while the attraction between the positive H and the electron-rich Y forces the X–H bond elongation.²² In general, the apparent reason of the frequency blue shifts is the X–H bond contraction; furthermore, there are no differences in nature between the proper red-shifted and improper blue-shifted HBs. In this work, we report a theoretical study of the unique HB interactions between boron hydride and π systems. Both red and blue shifts are predicted for the bridging hydrogen (H) atom (symmetric and asymmetric) stretching vibrations in the complexes.

Our interest in this new type of the HB interactions primarily stems from the discovery of an interaction between $n-B_{18}H_{22}$ and benzene in the molecular crystal where a bridging H atom of $n-B_{18}H_{22}$ directly interacts with benzene by facing the benzene centroid.²³ Hamilton et al. anticipated the presence of weak HBs between boron hydride and benzene according to the experimental results.²³ Distinctly different from the other (both proper and improper) HB interactions, in this case, the participants are the electron-poor boron hydride and the electron-rich π system. To elucidate the nature of this interaction, the prototype complex diborane–benzene was recently investigated by ab initio calculation analyses.²⁴ The authors suggested that the interactions between diborane and benzene should correspond to a unique region in the “hydrogen bond” map (see ref 24). The further characterization of this new class of complexes, in particular, red or blue shifts of frequency, was not available.²⁴ In the present study, three complexes consisting of the electron-deficient diborane (B_2H_6) and the electron-rich π systems [benzene (C_6H_6), 1,3-cyclopentadiene (C_5H_6), and cyclobuta-

* To whom correspondence should be addressed. E-mail: sxtian@ustc.edu.cn.

diene (C₄H₄)] are investigated with natural bond orbitals (NBO)²⁵ and atoms-in-molecules (AIM)^{26,27} electron topological analyses on the basis of the high-level ab initio calculations.

2. Methods and Calculations

The geometrical parameters of the complexes C_xH_y⋯B₂H₆ (*x*, *y* = 4, 5, or 6) and the related free monomers were fully optimized at the MP2²⁸/6-311++G(d, p) level of theory. In contrast to the previous calculations,²⁴ the basis set superposition error (BSSE) correction²⁹ was considered in the present geometrical optimizations of the complexes. The equilibrium structures were examined by the harmonic vibrational frequency calculations. The total energies were further calculated using the coupled-cluster CCSD(T) method in which the single, double, and triple excitations were included,³⁰ over the MP2 BSSE-corrected optimized geometries.

The NBO analysis transforms the canonical delocalized Hartree–Fock molecular orbitals (HF MOs) into the localized ones that are closely tied to chemical bond concepts. Filled NBOs describe the hypothetical, strictly localized Lewis structure. The interaction between filled bonding orbitals σ and vacant antibonding ones σ^* represents the deviation of the molecule from the Lewis structure and can be used as a measure of CT interactions (i.e., hyperconjugation or delocalization). Because the occupancies of bonding NBOs are highly condensed, the CT can be further treated by the second-perturbation energies $E(2)$,²⁵

$$E(2) = -n_{\sigma} \frac{\langle \sigma | F | \sigma^* \rangle^2}{\varepsilon_{\sigma^*} - \varepsilon_{\sigma}} = -n_{\sigma} \frac{F_{ij}^2}{\Delta\varepsilon} \quad (1)$$

where F_{ij} is the Fock matrix element between NBO *i* and *j*, ε_{σ} and ε_{σ^*} are the energies of σ and σ^* NBOs, and n_{σ} is the population. In this work, the MO wave functions obtained at the HF/6-311++G(d, p) level were used for the NBO analyses, for example, the hyperconjugative energies [$E(2)$, kcal/mol]. The other parameters regarding dipole moment and the hybridization at B atom were obtained at the same level of theory.

The topological features as far as the electron density $\rho(r)$ and its Laplace transform $\nabla^2\rho(r)$ at the critical points [CPs, where $\nabla\rho(r) = 0$] can be calculated with Bader's theory of AIM.^{26,27} The Laplacian of the charge density is defined as the sum of the three principal curvatures of the $\rho(r)$ function at each point in space

$$\nabla^2\rho_b = \frac{\partial^2\rho_b}{\partial x^2} + \frac{\partial^2\rho_b}{\partial y^2} + \frac{\partial^2\rho_b}{\partial z^2} = \lambda_1 + \lambda_2 + \lambda_3 \quad (2)$$

The Laplacian of the charge density at a point in space determines where the electronic charge is locally concentrated [$\nabla^2\rho(r) < 0$] or depleted [$\nabla^2\rho(r) > 0$].²⁶ There are four types of CPs: (3, -3), (3, -1), (3, +1), and (3, +3). Here, (3, -3), a true maximum, coincides with a nucleus position. When two neighboring atoms are chemically bonded to each other, a bond critical point (BCP) (3, -1) appears between them. At the BCP, the charge density is a minimum along the bond path but a maximum along any orthogonal displacement. (3, +1) corresponding to ring critical point (RCP) occurs in the interior of a bonded ring of atoms, and (3, +3), called the cage critical point (CCP), is a local minimum in $\rho(r)$ and can be found in the interior of a cage. For the complexes studied in this work, the values of ρ_b and $\nabla^2\rho_b$ at the (3, -1) BCPs, (3, +3) CCPs, and (3, +1) RCPs were calculated using the MP2/6-311++G(d, p) charge populations.

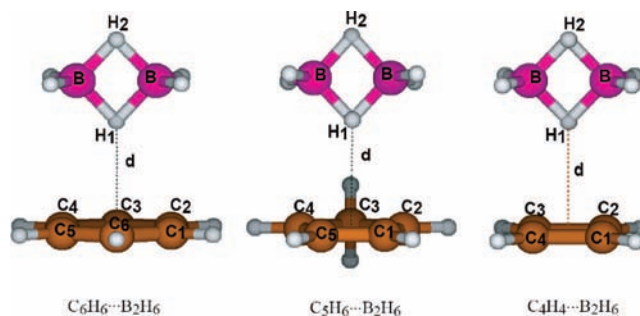
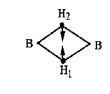
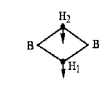


Figure 1. Schemes of the complexes. *d* represents the distance between the H1 atom and the centric point of the carbon ring.

TABLE 1: Geometry Parameters of the Free Monomer B₂H₆ and the Complexes C_xH_y⋯B₂H₆ (Bond Length in Å and Bond Angle in Deg), Interaction Energies (E_{int} in kcal/mol), and Frequency Shift (in cm⁻¹)

	C ₆ H ₆ ⋯B ₂ H ₆	C ₅ H ₆ ⋯B ₂ H ₆	C ₄ H ₄ ⋯B ₂ H ₆	B ₂ H ₆
Parameters ^a				
R(B–H ₁)	1.314 (1.314) ^a	1.313 (1.315)	1.311 (1.313)	1.315
R(B–H ₂)	1.319 (1.317)	1.319 (1.318)	1.319 (1.318)	1.315
R(B–B)	1.764 (1.762)	1.763 (1.764)	1.765 (1.765)	1.767
A(B–H ₁ –B)	84.34 (84.22)	84.34 (84.25)	84.59 (84.40)	84.37
A(B–H ₂ –B)	83.91 (84.00)	83.92 (84.02)	83.94 (84.03)	84.37
<i>d</i>	2.413 (2.590)	2.455 (2.596)	2.519 (2.653)	—
Interaction Energy ^b				
– $E_{\text{int}}^{\text{MP2+BSSE}}$	3.27	2.52	2.47	
– $E_{\text{int}}^{\text{CCSD(T)+BSSE}}$	2.45	2.41	1.83	
Frequencies ^c				
	2204.3 (–7.76)	2204.2 (–7.79)	2218.0 (+6.02)	2212.0
(sym-stretch)				
	2038.6 (+5.08)	2040.4 (+6.89)	2048.3 (+14.73)	2033.5
(asym-stretch)				

^a Values in the parentheses including the BSSE correction in the geometrical optimizations. ^b Over the MP2/6-311++G(d,p) optimized geometries. ^c Frequencies obtained without the BSSE correction. The frequency shifts upon the formation of the complexes are given in the parentheses.

The energetic and MO wave function calculations were performed with Gaussian 03.³¹ The AIM and NBO analyses were done with AIM2000³² and NBO 5.0 packages,³³ respectively.

3. Results and Discussion

3.1. Geometries of the Complexes and Interaction Energies.

Because of the much weaker interactions between diborane and π orbital,²⁴ the more sophisticated levels of theory are needed to achieve the equilibrium structures. Here, we pay more attention to the changes of intramolecular geometries upon the complex formations. The equilibrium structures of the complexes C₆H₆⋯B₂H₆, C₅H₆⋯B₂H₆, and C₄H₄⋯B₂H₆ are depicted in Figure 1. The geometrical parameters optimized by the MP2 and MP2 + BSSE methods are listed in Table 1.

The effects of complex formation on the structures of the monomers C_xH_y are found to be weak, on the basis of the results predicted at both the MP2 + BSSE and the MP2 levels. The carbon rings are expanded with 0.003, 0.001, and

TABLE 2: Topological Properties (in au) at the Critical Points of the Complexes $C_xH_y \cdots B_2H_6$ ^a

critical points	ρ_b				$\nabla^2\rho_b$				Hc			
	I	II	III	B ₂ H ₆	I	II	III	B ₂ H ₆	I	II	III	B ₂ H ₆
(3, -1) ^{1b}	0.1227	0.1224	0.1226	0.1211	-0.0324	-0.0323	-0.0332	-0.0339	-0.1012	-0.1009	-0.1010	-0.0992
(3, -1) ^{2b}	0.1212	0.1210	0.1208	0.1211	-0.0321	-0.0317	-0.0317	-0.0339	-0.0994	-0.0992	-0.0991	-0.0992
(3, -1) ^{3b}	0.0059	0.0070	0.0070		0.0204	0.0203	0.0182		0.0007	0.0007	0.0008	
(3, +1) ^{1r}	0.1155	0.1152	0.1151	0.1146	0.0132	0.0130	-0.0128	0.0122	-0.0646	0.0643	-0.0641	-0.0635

^a I, II, and III represent the complexes C₆H₆⋯B₂H₆, C₅H₆⋯B₂H₆, and C₄H₄⋯B₂H₆, respectively.

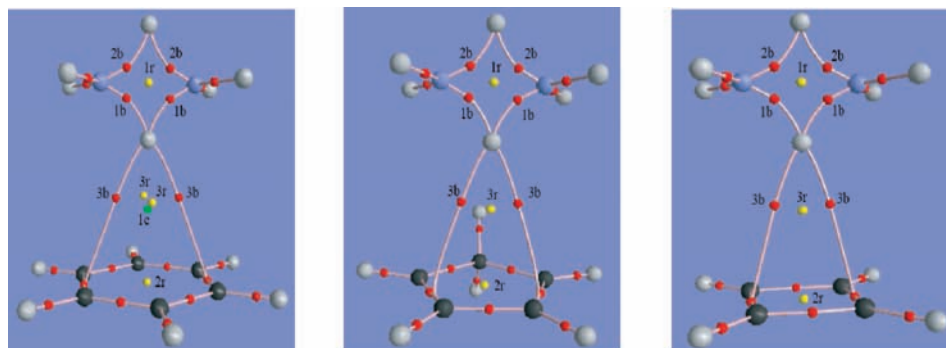


Figure 2. Electron topological analyses for the complexes (from left to right): C₆H₆⋯B₂H₆, C₅H₆⋯B₂H₆, and C₄H₄⋯B₂H₆. The bond (red circles), ring (yellow circles), and cage (green circle) critical points are denoted b, r, and c, respectively.

0.001 Å for C₆H₆, C₅H₆, and C₄H₄, respectively. In comparison with the free monomer B₂H₆, the geometrical variances of the diborane moiety in the complexes are observed; namely, the MP2 optimizations without the BSSE corrections indicate that the bond lengths of B–H₁ are shortened by 0.001, 0.002, and 0.004 Å for the complexes C₆H₆⋯B₂H₆, C₅H₆⋯B₂H₆, and C₄H₄⋯B₂H₆, respectively; all of the bond lengths of B–H₂ are elongated by 0.004 Å. The peripheral B–H bonds in diborane are almost unaffected by the formation of the complexes, showing that the bond length changes less than 0.001 Å. With the BSSE corrections, the MP2 optimizations predict similar results. The distances “d” between the H₁ atom in diborane and the centers of the carbon rings are 2.413, 2.455, and 2.519 Å predicted at the MP2 level, while they are 2.590, 2.596, and 2.653 Å at the MP2 + BSSE level for the complexes C₆H₆⋯B₂H₆, C₅H₆⋯B₂H₆, and C₄H₄⋯B₂H₆, respectively. Therefore, the BSSE corrections lead to the larger equilibrium distances. Such a BSSE correction effect has been pointed out in ref 29. The longer distance (2.590 Å) corrected by the BSSE effect in the C₆H₆⋯B₂H₆ complex is closer to the experimental data 2.74–3.00 Å (the distance between polyhedral boron and benzene in the crystal).²³ The higher-level approach of geometrical optimization such as the CCSD(T) level of theory with the BSSE correction is currently too computationally demanding to be available.

Over the MP2 + BSSE optimized geometries, the interaction energies (E_{int}) together with the standard BSSE-corrected³⁴ values were obtained at the CCSD(T) and MP2 levels of theory. As shown in Table 1, these two methods predict a consistent order of E_{int} values: The strongest one is of C₆H₆⋯B₂H₆, while the weakest is of C₄H₄⋯B₂H₆. The present E_{int} values fall in the weak HB energy scale, which is close to the van der Waals complex region (see Figure 7 in ref 6). Li et al. have pointed out that the dispersive force was predominant in the interaction between C₆H₆ and B₂H₆.²⁴ Our extended calculations also show that the dispersive force is the strongest attraction around the equilibrium structures of these three complexes.³⁵

It is surprising that in comparison with two vibrational modes (symmetric and asymmetric stretching of the bridging

TABLE 3: NBO Analyses of the Different Properties of the Complexes $C_xH_y \cdots B_2H_6$ in Comparison with the Free Diborane

parameters	C ₆ H ₆ ⋯B ₂ H ₆	C ₅ H ₆ ⋯B ₂ H ₆	C ₄ H ₄ ⋯B ₂ H ₆	B ₂ H ₆
q(B) ^a	0.0306	0.0297	0.0290	0.0297
q(H ₁) ^a	0.0426	0.0421	0.0410	0.0417
q(H ₂) ^a	0.0362	0.0362	0.0360	0.0417
q(CT) ^b	0.0146	0.0167	0.0194	
sp ⁿ (BH ₁ B) ^c	sp ^{4.36}	sp ^{4.37}	sp ^{4.38}	sp ^{4.61}
% s-character ^d	18.55	18.52	18.48	17.73
sp ⁿ (BH ₂ B) ^c	sp ^{4.73}	sp ^{4.74}	sp ^{4.74}	sp ^{4.61}
% s-character ^d	17.37	17.32	17.33	17.73
μ (B ₂ H ₆) ^e	0.29	0.27	0.25	0.00

^a Natural atomic population (electron unit). ^b Transferred charge from C_xH_y to diborane (electron unit). ^c The hybridization at B atom in the 3c-2e τ_{BHB} bond. ^d The percent of the s-character for the B atom. ^e μ represents the dipole moment (in Debye).

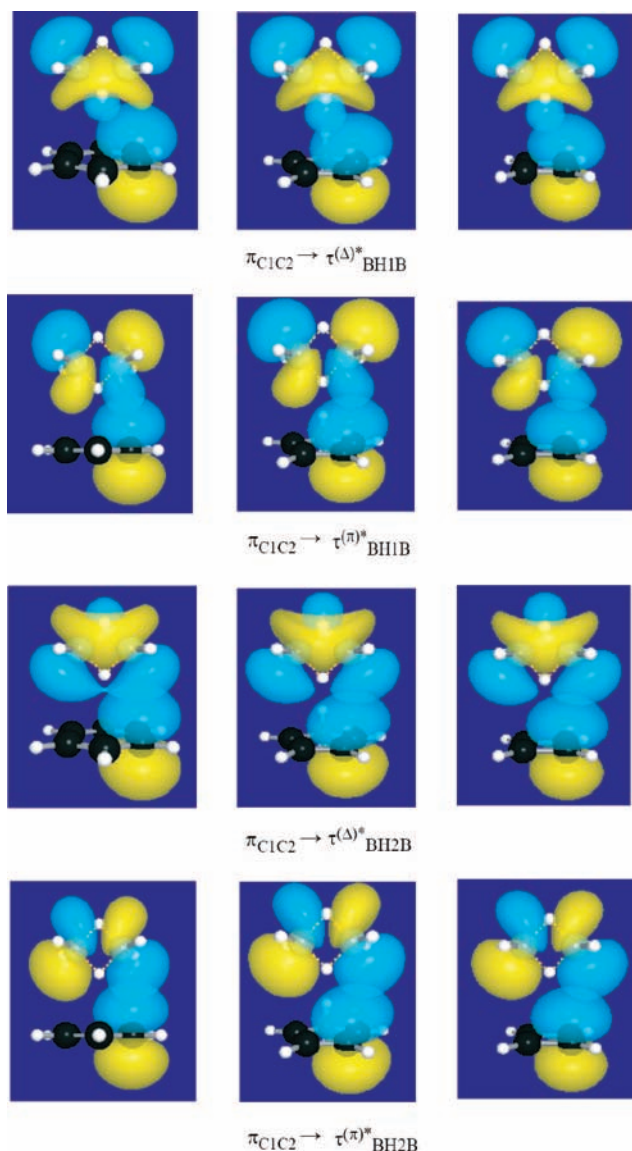
H atoms; see the schemes in Table 1) of the free monomer B₂H₆, the different values of blue shifts for the asymmetric stretching and the variance from the red shifts to a blue shift for the symmetric stretching are predicted for these three complexes. No studies about the vibrational frequency shifts of these systems are reported prior to this work. More insights into the frequency shifts will be presented in the following text. Moreover, the characteristics of the interactions in these complexes, that is, whether they are the hydrogen-bonded complexes, are still unclear, although their interaction energies fall in the weak HB energy scale.

3.2. Electron Topological Analyses. A proof for the existence of HB is the identification of the BCPs between the H atom and the HB acceptor. In Table 2, the values of ρ_b and $\nabla^2\rho_b$ of the complexes are compared with those of the free monomers in detail. Figure 2 shows the distributions of the critical point BCPs (red circles), RCPs (yellow circles), and CCPs (green circle) in the complexes, denoted as (3, -1)^b, (3, +1)^r, and (3, +3)^c in the text, respectively. One can find that in the complexes there exist BCPs (3, -1)^{3b} and RCP (3, +1)^{3r} between the subsystems; furthermore, there is a CCP (3, +3)^{1c} for C₆H₆⋯B₂H₆. In C₆H₆⋯B₂H₆ and C₄H₄⋯B₂H₆, the bond paths of (3, -1)^{3b} link the bridging

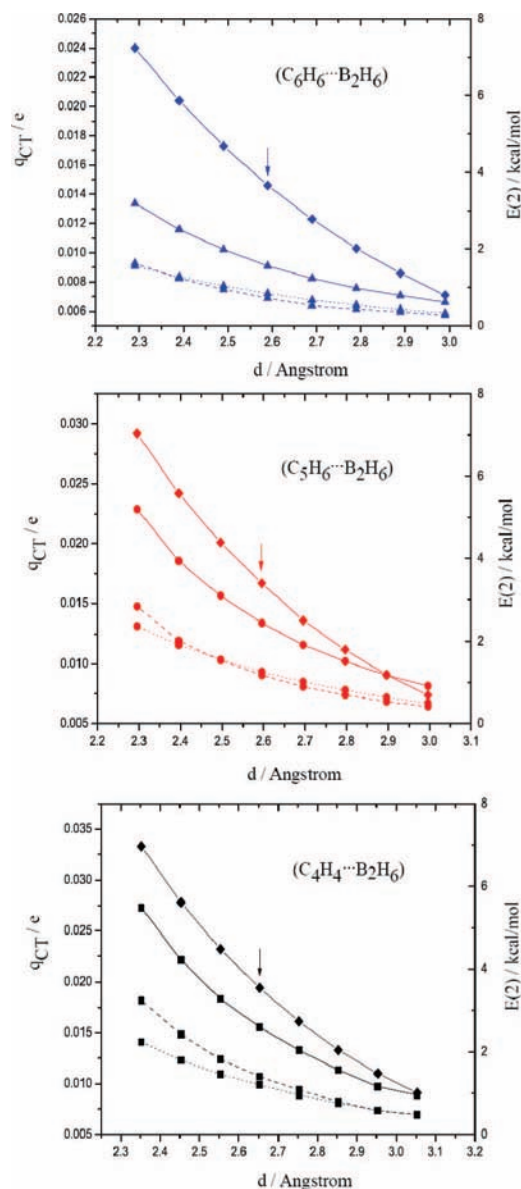
TABLE 4: Predominant Hyperconjugative Interaction (i.e., CT) Energies of the Complexes $C_xH_y \cdots B_2H_6^a$

donor ^b	acceptor ^c	$\delta\epsilon$ (au)			F_{ij} (au)			$E(2)$ (kcal/mol)		
		I	II	III	I	II	III	I	II	III
π_{C1C2}	$\tau_{BH1B}^{(\Delta)*}$	0.88	0.92	0.95	0.003	0.007	0.009	0.01	0.06	0.11
	$\tau_{BH1B}^{(\pi)*}$	0.67	0.71	0.74	0.016	0.018	0.019	0.41	0.53	0.59
	$\tau_{BH2B}^{(\Delta)*}$	0.86	0.90	0.92	0.013	0.014	0.013	0.21	0.25	0.22
	$\tau_{BH2B}^{(\pi)*}$	0.67	0.71	0.74	0.015	0.015	0.015	0.33	0.38	0.38

^a I, II, and III represent the complexes $C_6H_6 \cdots B_2H_6$, $C_5H_6 \cdots B_2H_6$, and $C_4H_4 \cdots B_2H_6$, respectively. ^b According to the symmetry, for $C_6H_6 \cdots B_2H_6$, the interaction for $\pi_{C3C4} \rightarrow \tau_{BH1(2)B}^*$ is the same with $\pi_{C5C6} \rightarrow \tau_{BH1(2)B}^*$ (τ_{BHB}^* including $\tau_{BHB}^{(\pi)*}$ and $\tau_{BHB}^{(\Delta)*}$); $E(2)$ for $\pi_{C3C4} \rightarrow \tau_{BH1B}^*$ and $\pi_{C3C4} \rightarrow \tau_{BH2B}^*$ are both 0.15 kcal/mol ($F_{ij} \sim 0.015$ and 0.014 au, respectively); for $C_5H_6 \cdots B_2H_6$, $\pi_{C4C5} \rightarrow \tau_{BH1(2)B}^*$ are the same with $\pi_{C1C2} \rightarrow \tau_{BH1(2)B}^*$, and for $C_4H_4 \cdots B_2H_6$, $\pi_{C3C4} \rightarrow \tau_{BH1(2)B}^*$ are the same with $\pi_{C1C2} \rightarrow \tau_{BH1(2)B}^*$. ^c $\tau^{(\Delta)*}$ and $\tau^{(\pi)*}$ represent the anti 3c-2e bonds.

**Figure 3.** Hyperconjugative interactions (from the left to right panels): $C_6H_6 \cdots B_2H_6$, $C_5H_6 \cdots B_2H_6$, and $C_4H_4 \cdots B_2H_6$.

hydrogen atom H_1 to one of the carbon–carbon BCPs, which is related to the “conflict catastrophe structure”.²⁶ In these two complexes, the $(3, -1)$ BCP in the carbon–carbon bond is an attractor for the bond path linking the H_1 atom to this carbon–carbon bond. On the other hand, in $C_5H_6 \cdots B_2H_6$, although the bond path of the $(3, -1)^{3b}$ links the bridging H_1 atom to one of the carbon atoms, this bond path almost passes through the $(3, -1)$ BCP of the carbon–carbon bond (see Figure 2). As shown in Table 2, ρ_b [0.0059–0.0070 au

**Figure 4.** Correlations of the total CT q_{CT} (diamond connected with solid line in different colors) or the total $E(2)$ values for $\pi \rightarrow \tau_{BH1B}^*$ (broken line), $\rightarrow \tau_{BH2B}^*$ (dotted line), and \rightarrow total τ_{BHB}^* (solid line) for $C_6H_6 \cdots B_2H_6$ (blue triangles), $C_5H_6 \cdots B_2H_6$ (red circles), and $C_4H_4 \cdots B_2H_6$ (black squares) with scanning the distances between two molecular moieties. The arrows point to the equilibrium structures.

at $(3, -1)^{3b}$] and their $\nabla^2\rho_b$ (0.0182–0.0204 au) are well-satisfied with the criteria for the existence of HBs.²⁷

The local energy densities at the BCPs provide valuable information to explore the nature of an interaction:

$$H_C = G_C - V_C \quad (3)$$

Here, H_C is the total energy density, and G_C and V_C are the kinetic and potential energy densities at the BCPs, respectively. The H_C characterizes the type of bond: The positive values of H_C are found in the ionic bonds and HBs, while the negative H_C is found for the covalent interactions.^{26,27} For the present complexes, the

positive values of H_C at the $(3, -1)^{3b}$ also indicate the existence of the weak HB, although these H_C values, 0.0007 and 0.0008 au, are extremely small. In general, the much lower values of ρ_b , $\nabla^2\rho_b$, and H_C imply that the interactions between diborane and π orbitals are extremely weak. However, the HB characteristics of the interactions in these complexes are definitely confirmed for the first time with AIM electron topological analyses.

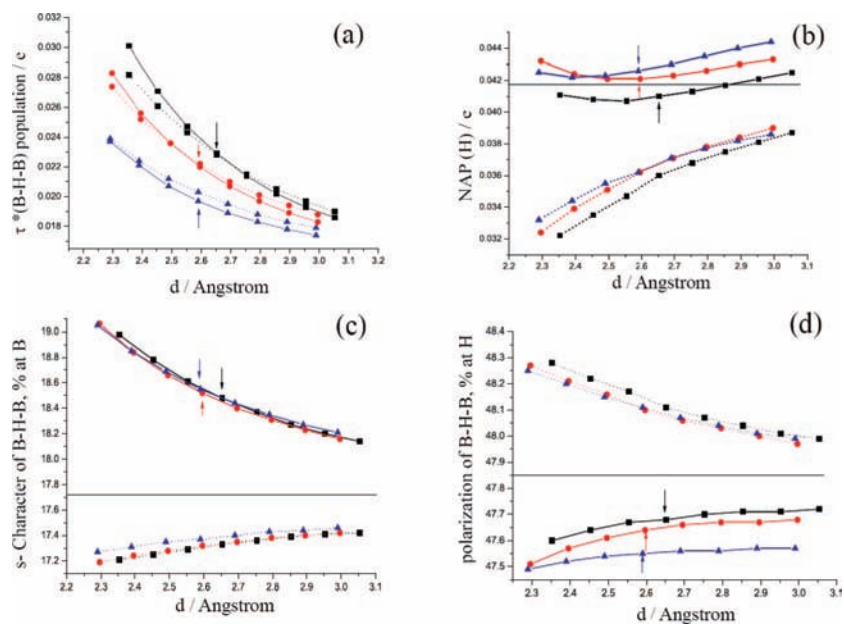


Figure 5. Correlations of the τ_{BHB}^* population (a), natural atomic population of the bridging H atom (b), the percent of B-centered s-character of the B–H–B bond (c), or the percent of polarization of the B–H–B bond at H or B atom for scanning the distances between two molecular moieties: $\text{C}_6\text{H}_6 \cdots \text{B}_2\text{H}_6$ (blue triangles), $\text{C}_5\text{H}_6 \cdots \text{B}_2\text{H}_6$ (red circles), and $\text{C}_4\text{H}_4 \cdots \text{B}_2\text{H}_6$ (black squares). For B–H1–B, solid line; B–H2–B, broken line. The arrows point to the equilibrium structures. In panels b–d, the horizontal lines represent the values of the free monomer B_2H_6 .

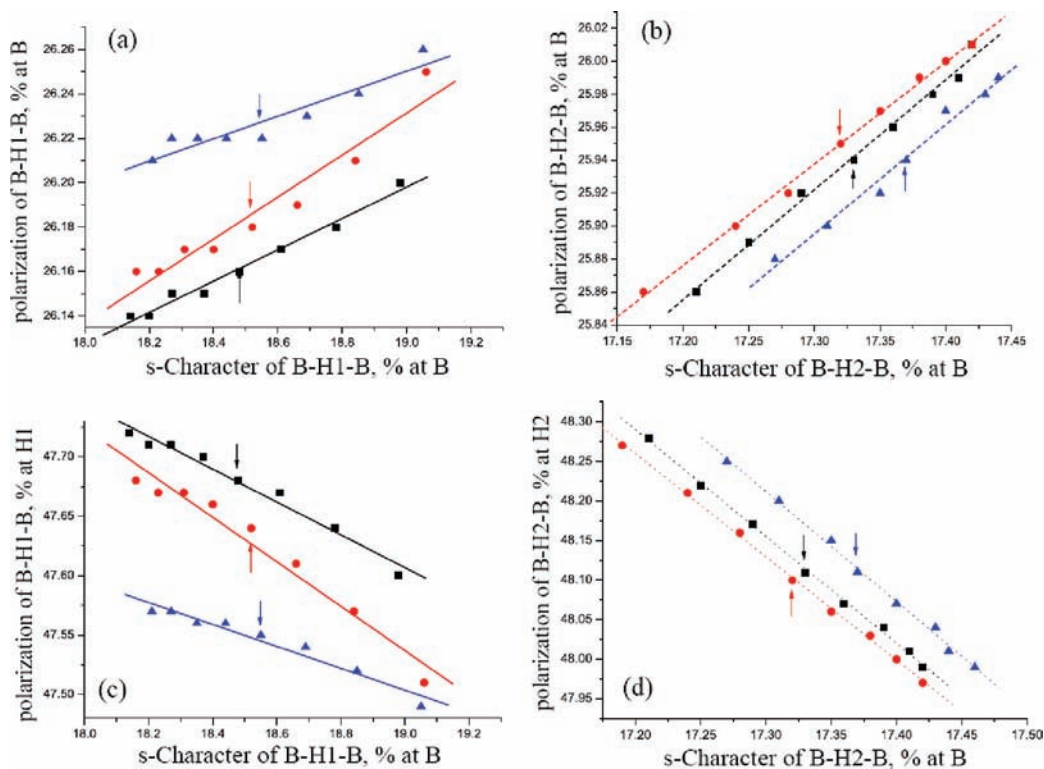


Figure 6. Correlations of the percent of polarization of the B–H–B bond at H or B atom and the percent of s-character at the B-centered hybrid in this bond for scanning the distances between two molecular moieties: $\text{C}_6\text{H}_6 \cdots \text{B}_2\text{H}_6$ (blue triangles), $\text{C}_5\text{H}_6 \cdots \text{B}_2\text{H}_6$ (red circles), and $\text{C}_4\text{H}_4 \cdots \text{B}_2\text{H}_6$ (black squares). The arrows point to the equilibrium structures.

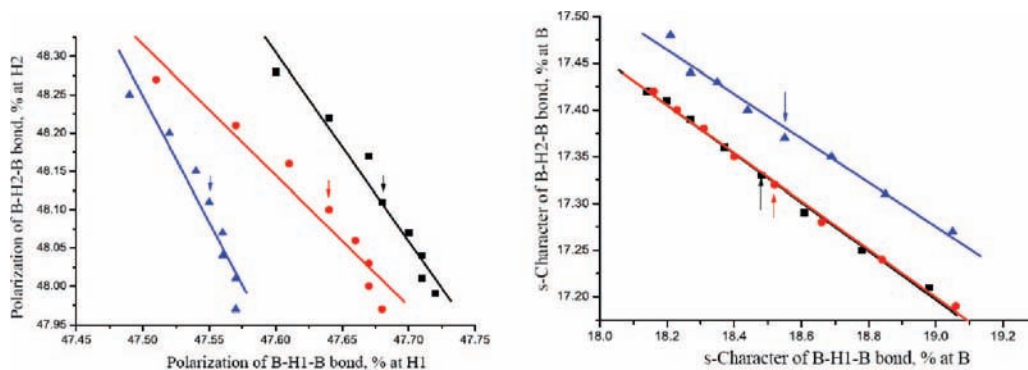


Figure 7. Correlations of the percent of polarization of two B–H–B bonds at H atoms (left) and correlation of the percent of s-character at the B-centered hybrids (right) for scanning the distances between two molecular moieties: C₆H₆···B₂H₆ (blue triangles), C₅H₆···B₂H₆ (red circles), and C₄H₄···B₂H₆ (black squares). The arrows point to the equilibrium structures.

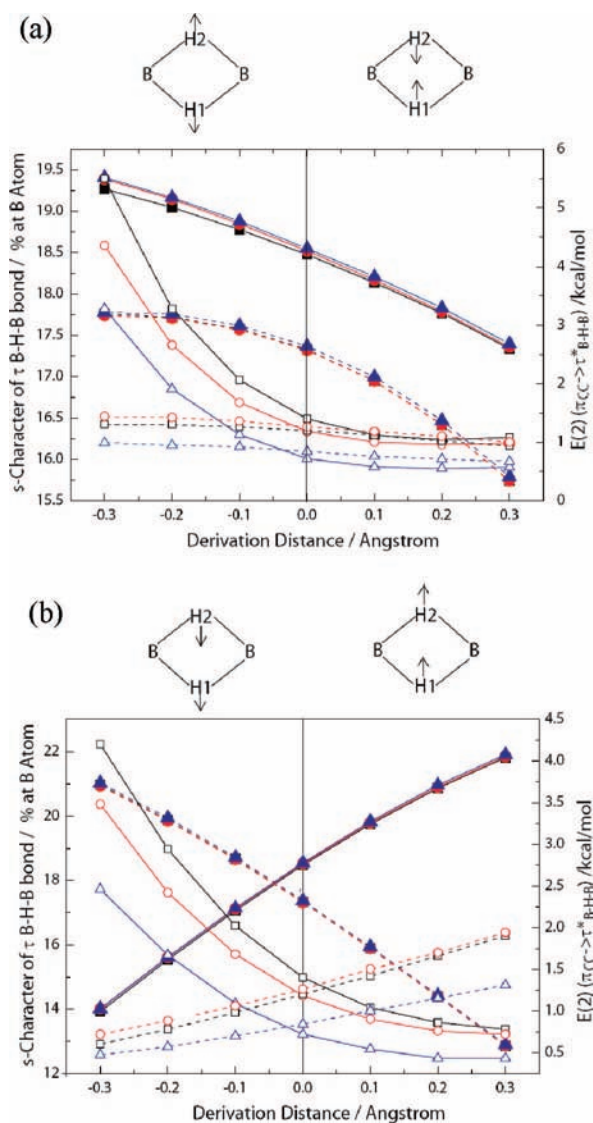


Figure 8. Correlations of the percent of s-character at the B-centered hybrid (solid symbols, B–H₁–B with solid line; B–H₂–B, with broken line) or $E(2)$ energies (open symbols) and derivation distances along the symmetric (a) and asymmetric (b) vibrations: C₆H₆···B₂H₆ (triangles), C₅H₆···B₂H₆ (circles), and C₄H₄···B₂H₆ (squares).

3.3. NBO Analyses and Vibrational Frequency Shifts.

Distinctly different from both the proper and the improper HB complexes, here, the HB donor component of the complexes is the electron-deficient molecule B₂H₆. A certain amount of

electron density can be readily transferred from the electron-rich molecules C_xH_y to B₂H₆.

The NBO analyses such as natural atomic populations (NAP, q), CT quantity [noted as $q(\text{CT})$], hybridization of B atoms in the so-called three-center two-electron (3c-2e) B–H–B,²⁵ and CT or hyperconjugation energies are listed in Tables 3 and 4. The NAP values $q(\text{B})$, $q(\text{H}_1)$, and $q(\text{H}_2)$ in the complexes are different from them in the free monomer B₂H₆: $q(\text{B})$ is larger in C₆H₆···B₂H₆, while it is smaller in C₄H₄···B₂H₆ than that in B₂H₆; $q(\text{H}_1)$ values increase in C₆H₆···B₂H₆ and C₅H₆···B₂H₆ but decrease in C₄H₄···B₂H₆; all $q(\text{H}_2)$ values in the complexes are smaller than that in B₂H₆. A sequence of $q(\text{CT})$ values, 0.0194 e (C₄H₄···B₂H₆) > 0.0167 e (C₅H₆···B₂H₆) > 0.0146 e (C₆H₆···B₂H₆), is in line with the ionization energy order of the HB acceptors, 8.16 eV (C₄H₄) < 8.44 eV (C₅H₆) < 9.24384 eV (C₆H₆),³⁶ indicating that the lower ionization energies lead to the more negative charges transferred from the hydrocarbons. The different stereo CT processes occurring between the hydrocarbon π and the diborane 3c-2e empty $\tau(\Delta)^*$ and $\tau(\pi)^*$ orbitals, are depicted in Figure 3. According to the $E(2)$ values in Table 4, the CT (i.e., hyperconjugative) interaction energies for $\pi \rightarrow \tau_{\text{BH1B}}^*$ ($\tau(\Delta)^* + \tau(\pi)^*$) are 0.72, 1.18, and 1.40 kcal/mol for C₆H₆···B₂H₆, C₅H₆···B₂H₆, and C₄H₄···B₂H₆, respectively; their respective $\pi \rightarrow \tau_{\text{BH2B}}^*$ interaction energies are 0.84, 1.26, and 1.20 kcal/mol. Apparently, the hyperconjugative interactions for the τ^* orbitals near the hydrocarbon are weaker than those for the remote τ^* orbitals in the former two complexes, while it is reversed for C₄H₄···B₂H₆. These findings will be used in an understanding of the vibrational frequency shifts.

Before going into the details, we recall the arguments on the interpretations to the improper blue-shifted HBs. A subtle balance between hyperconjugation and rehybridization was established by Alabugin et al.²¹ on the basis of Bent's rule.³⁷ However, there is a operation difficulty to find the accurate balance where red- and blue-shifted HBs can be distinguished.^{21,22} Joseph and Jemmis, based on the simple electrostatic interactions, concluded that for all X–H···Y, the electron affinity of X caused electron attraction from Y and led to the X–H bond contraction (i.e., blue shift of X–H stretching), while the X–H bond elongation (i.e., red shift) was due to the electrostatic attraction between H and Y atoms.²² Within the above two schemes, for this case, it is easy to interpret the geometrical variances of the complexes with respect to the free monomers (see Table 1). Although the transferred charges from π orbitals to $\tau_{\text{BH1(2)B}}^*$ are different, the negative-charged carbon atoms in C_xH_y attract the near positive-charged 3c-2e B–H₁–B bond more strongly than the remote B–H₂–B bond. This attraction

results in the electron density redistributions; finally, the electron-deficient τ_{BH1B} bond is strengthened. The shorter B–H₁ distances and the wider B–H₁–B angle (see Table 1) are the manifestations of this process.

The predicted blue shifts of asymmetric stretching vibrations in the complexes can not be simply interpreted by the B–H₁ distance shortening or τ_{BH1B} strengthening, because both B–H₁–B and B–H₂–B are involved in this vibrational mode. On the other hand, it is necessary to explore the mechanism that the blue shift 6.02 cm⁻¹ of symmetric stretching of C₄H₄•••B₂H₆ is dramatically different from the red shifts -7.76 cm⁻¹ of C₆H₆•••B₂H₆ and -7.79 cm⁻¹ of C₅H₆•••B₂H₆.

Following the discussion of Alabugin et al.,²¹ an increase of the s-character in hybrid orbital X–H (i.e., at X atom) is associated with this bond shortening; contrarily, the hyperconjugative interaction $n(\text{Y}) \rightarrow \sigma_{\text{XH}}^*$ induces the X–H lengthening. The increase of the s-character of X atom also leads to the simultaneous increase in the p-character of other bonds connected to X atom, namely, a rehybridization or repolarization process, which, as proposed by Hobza and Havlas,¹² can explain the structural reorganizations (usually leading to the other X-connected bond elongation).

As shown in Figure 4, at the shorter distances between two molecular moieties in the complexes, the increase of the orbital overlap between π and τ_{BHB}^* (see Figure 3) leads to the increase of $E(2)$ values and the CT quantities q_{CT} . The HB effects on two B–H–B parts can be clearly observed in Figure 5, where the d -dependence correlations of τ_{BHB}^* orbital and H1(2) atomic populations, the percents of B-centered s-character, and polarization at H1(2) atom in the τ_{BHB} bond are depicted. In Figure 5a, the more transferred charge occupies on the τ_{BHB}^* orbital when two molecular moieties approach to each other. In Figure 5b–d, the trends of NPA of H1 atom, s-character of the B atom, and polarization of the H1 atom in the B–H₁–B bond are reverse to those in B–H₂–B bond, indicating that the dynamics of repolarizations or rehybridizations on B–H₁–B should be different from that on B–H₂–B although their CT processes or hyperconjugative interactions are similar. The correlations between the s-character and the polarization in the same B–H–B bond are depicted in Figure 6. Combined with Figure 5, one can find that at the longer distances the percents both of s-character and polarization at B atom decrease and the percents of polarization at H1 atom in B–H₁–B bond increase, but the totally reverse trends are found for the B–H₂–B bond. Whatever, these strong correlations between the bond polarization and the rehybridization (i.e., s-character percent) are similar to the blue-shifted complexes CHF₃•••H₂O or chloride anion (see Figure 9 of ref 21). In the complexes C_xH_y•••B₂H₆, only the bridging H1 atom is directly involved in the HB interactions. However, the above analyses (from Figures 4 to 6) indicate that both of the two B–H–B bonds should be related to the HB interactions. This is further proved in Figure 7, where the polarization of two bridging H atoms (Figure 7a) and the percents of s-character at B atoms (Figure 7b) are highly correlated. This is in line with the conclusions about the well-known mechanism of the blue-shifted HB interactions.^{12,21}

To elucidate the reason that the frequency shifts of symmetric H stretching model are different from the asymmetric shifts, we also plotted the changes of the percent of s-character of the B atom and $E(2)$ energies in terms of the geometrical variances around the equilibrium structures along symmetric (in Figure 8a) and asymmetric (in Figure 8b) vibrations. In Figure 8a (symmetric vibration), with the reference to the H1 atom position, when the H1 atom approaches to hydrocarbons (the

negative derivation distance shown in Figure 8), both the B-atom s-character in the B–H₁–B bond and $E(2)$ of $\pi \rightarrow \tau_{\text{BH1B}}^*$ interactions increase, and they decrease rightabout; the $E(2)$ values of $\pi \rightarrow \tau_{\text{BH2B}}^*$ interactions vary only in a small scale. In Figure 8b (asymmetric vibration), the changes of the B-atom s-character in the B–H₁–B bond and $E(2)$ of $\pi \rightarrow \tau_{\text{BH2B}}^*$ interactions dramatically differ from those for the symmetric vibration shown in Figure 8a. If the blue shifts of the asymmetric stretching mode 5.08 cm⁻¹ of C₆H₆•••B₂H₆, 6.89 cm⁻¹ of C₅H₆•••B₂H₆, and 14.73 cm⁻¹ of C₄H₄•••B₂H₆ are interpreted solely that the rehybridization (i.e., s-character of B atom or repolarization) surmounts hyperconjugation in the B–H₁–B bond shown in Figure 8a, this balance mechanism will meet with the fateful difficulties in the interpretation to the red shifts -7.76 cm⁻¹ in C₆H₆•••B₂H₆ and -7.79 cm⁻¹ in C₅H₆•••B₂H₆ but the blue shift 6.02 cm⁻¹ in C₄H₄•••B₂H₆ for the symmetric vibrations. Further studies to reasonably interpret such frequency shifts are still in progress in our laboratory. The spectroscopic experimental studies, for example, infrared and Raman spectroscopy, on these complexes are expected.

4. Concluding Remarks

A new type of HB interactions in C₆H₆•••B₂H₆, C₅H₆•••B₂H₆, and C₄H₄•••B₂H₆ is identified on the basis of AIM and NBO analyses combined with the high-level ab initio calculations. The HB interaction strengths are in the order of C₆H₆•••B₂H₆ > C₅H₆•••B₂H₆ > C₄H₄•••B₂H₆, contrary to a sequence of transferred charges 0.0194 e (C₄H₄•••B₂H₆) > 0.0167 e (C₅H₆•••B₂H₆) > 0.0146 e (C₆H₆•••B₂H₆), which is interpreted by the predominant dispersive (not electrostatic) forces to stabilize the complexes. For two vibrational modes of the bridging H-atom stretching in the complexes as compared with those of the free monomer B₂H₆, the theoretical calculations predict two frequency red shifts, -7.76 cm⁻¹ of C₆H₆•••B₂H₆ and -7.79 cm⁻¹ of C₅H₆•••B₂H₆, and a blue shift, 6.02 cm⁻¹ of C₄H₄•••B₂H₆, for the symmetric stretching, while three blue shifts, 5.08 cm⁻¹ of C₆H₆•••B₂H₆, 6.89 cm⁻¹ of C₅H₆•••B₂H₆, and 14.73 cm⁻¹ of C₄H₄•••B₂H₆, are predicted for the asymmetric stretching.

To the best of our knowledge, no such blue- or red-shifted vibrations for these complexes have been studied prior to this work. Distinctly different from the local stretching vibrational mode of a single bond, the complexity and variety of the blue- or red-shifted multiple-bond stretching vibrations will be a challenge toward a complete understanding of HB effects.

Acknowledgment. This work is supported by NSFC (Grant No. 20673105), MOST Natural Basic Research Program of China (Grant No. 2006CB922004), MOST 973 program (Grant No. 2007CB815204), and the NCET program of the Ministry of Education of China.

References and Notes

- (1) (a) Pimentel, G. C.; McClellan, A. L. *The Hydrogen Bond*; W. H. Freeman: San Francisco, CA, 1960. (b) Joesten, M. D.; Schaad, L. J. *Hydrogen Bonding*; Marcel Dekker: New York, 1974. (c) Jeffrey, G. A. *An Introduction to Hydrogen Bonding*; Oxford University Press: New York, 1997. (d) Scheiner, S. *Hydrogen Bonding. A Theoretical Perspective*; Oxford University Press: Oxford, 1997. (e) Desiraju, G. R.; Steiner, T. *The Weak Hydrogen Bond in Structural Chemistry and Biology*; Oxford University Press: Oxford, 1999. (f) Steiner, T. *Angew. Chem., Int. Ed. Engl.* **2002**, *41*, 48.
- (2) Pauling, L. *The Nature of the Chemical Bond*; Cornell University Press: Ithaca, NY, 1939.
- (3) Umeyama, H.; Morokuma, K. *J. Am. Chem. Soc.* **1977**, *99*, 1316.
- (4) Ratajczak, H. *J. Phys. Chem.* **1972**, *76*, 3000.
- (5) Tichy, M. *Adv. Org. Chem.* **1965**, *5*, 115.

- (6) Desiraju, G. R. *Acc. Chem. Res.* **2002**, *35*, 565.
- (7) Hunter, C. A. *Chem. Soc. Rev.* **1994**, *23*, 101.
- (8) Dougherty, D. A. *Science* **1996**, *271*, 163.
- (9) Nishio, M.; Hirota, M.; Umezawa, Y. *The CH/π Interaction: Evidence, Nature and Consequences*; Wiley-VCH: Weinheim, 1998.
- (10) Caminati, W.; Melandri, S.; Moreschini, P.; Favero, P. G. *Angew. Chem., Int. Ed. Engl.* **1999**, *38*, 2924.
- (11) Van der Veken, B. J.; Herrebout, W. A.; Szostak, R.; Shchepkin, D. N.; Havlas, Z.; Hobza, P. *J. Am. Chem. Soc.* **2001**, *123*, 12290.
- (12) Hobza, P.; Havlas, Z. *Chem. Rev.* **2000**, *100*, 4253.
- (13) Li, X. S.; Liu, L.; Schlegel, H. B. *J. Am. Chem. Soc.* **2002**, *124*, 9639.
- (14) Grabowski, S. J., Ed. *Hydrogen Bonding—New Insights*; Springer: Dordrecht, The Netherlands, 2006; see references therein.
- (15) Pejov, L.; Hermansson, K. *J. Chem. Phys.* **2003**, *119*, 313.
- (16) Hobza, P.; Havlas, Z. *Theor. Chem. Acc.* **2002**, *108*, 325.
- (17) Hobza, P. *Phys. Chem. Chem. Phys.* **2001**, *3*, 2555.
- (18) Zierkiewicz, W.; Michalska, D.; Havlas, Z.; Hobza, P. *Chem. Phys. Chem.* **2002**, *3*, 511.
- (19) Masunov, A.; Dannenberg, J. J.; Contreras, R. H. *J. Phys. Chem. A* **2001**, *105*, 4737.
- (20) Hermansson, K. *J. Phys. Chem. A* **2002**, *106*, 4695.
- (21) Alabugin, I. V.; Manoharan, M.; Peabody, S.; Weinhold, F. *J. Am. Chem. Soc.* **2003**, *125*, 5973.
- (22) Joseph, J.; Jemmis, E. D. *J. Am. Chem. Soc.* **2007**, *129*, 4620.
- (23) Hamilton, E. J. M.; Kultyshev, R. G.; Du, B.; Meyers, E. A.; Liu, S.; Hadad, C. M.; Shore, S. G. *Chem. Eur. J.* **2006**, *12*, 2571.
- (24) Li, H. Z.; Min, D. H.; Shore, S. G.; Lipscomb, W. N.; Yang, W. *Inorg. Chem.* **2007**, *46*, 3956.
- (25) Weinhold, F.; Landis, C. *Valency and Bonding*; Cambridge University Press: Cambridge, 2005.
- (26) Bader, R. F. W. *Atoms in Molecules: A Quantum Theory*; Clarendon: Oxford, 1990.
- (27) Popelier, P.; *Atoms in Molecules: An Introduction*; Prentice-Hall: Harlow, 2000.
- (28) Head-Gordon, M.; Pople, J. A.; Frisch, M. J. *Chem. Phys. Lett.* **1988**, *153*, 503.
- (29) Simon, S.; Duran, M.; Dannenberg, J. J. *J. Chem. Phys.* **1996**, *105*, 11024.
- (30) (a) Cizek, J. *Adv. Chem. Phys.* **1969**, *14*, 35. (b) Pople, J. A.; Krishnan, R.; Schlegel, H. B.; Binkley, J. S. *Int. J. Quantum Chem.* **1978**, *14*, 545. (c) Bartlett, R. J.; Purvis, G. D. *Int. J. Quantum Chem.* **1978**, *14*, 516.
- (31) Frisch, M. J.; Trucks, G. W.; Schlegel, H. B.; Scuseria, G. E.; Robb, M. A.; Cheeseman, J. R.; Montgomery, J. A., Jr.; Vreven, T.; Kudin, K. N.; Burant, J. C.; Millam, J. M.; Iyengar, S. S.; Tomasi, J.; Barone, V.; Mennucci, B.; Cossi, M.; Scalmani, G.; Rega, N.; Petersson, G. A.; Nakatsuji, H.; Hada, M.; Ehara, M.; Toyota, K.; Fukuda, R.; Hasegawa, J.; Ishida, M.; Nakajima, T.; Honda, Y.; Kitao, O.; Nakai, H.; Klene, M.; Li, X.; Knox, J. E.; Hratchian, H. P.; Cross, J. B.; Adamo, C.; Jaramillo, J.; Gomperts, R.; Stratmann, R. E.; Yazyev, O.; Austin, A. J.; Cammi, R.; Pomelli, C.; Ochterski, J. W.; Ayala, P. Y.; Morokuma, K.; Voth, G. A.; Salvador, P.; Dannenberg, J. J.; Zakrzewski, V. G.; Dapprich, S.; Daniels, A. D.; Strain, M. C.; Farkas, O.; Malick, D. K.; Rabuck, A. D.; Raghavachari, K.; Foresman, J. B.; Ortiz, J. V.; Cui, Q.; Baboul, A. G.; Clifford, S.; Cioslowski, J.; Stefanov, B. B.; Liu, G.; Liashenko, A.; Piskorz, P.; Komaromi, I.; Martin, R. L.; Fox, D. J.; Keith, T.; Al-Laham, M. A.; Peng, C. Y.; Nanayakkara, A.; Challacombe, M.; Gill, P. M. W.; Johnson, B.; Chen, W.; Wong, M. W.; Gonzalez, C.; Pople, J. A. *Gaussian 03*; Gaussian, Inc.: Pittsburgh, PA, 2003.
- (32) AIM 2000: A Program to Analyze and Visualize Atoms in Molecules; see <http://www.aim2000.de/>.
- (33) Glendening, E. D.; Badenhoop, J. K.; Reed, A. E.; Carpenter, J. E.; Bohmann, J. A.; Morales, C. M.; Weinhold, F. *NBO 5.0*; Theoretical Chemistry Institute, University of Wisconsin: Madison, WI, 2001.
- (34) Boys, S. F.; Bernardi, F. *Mol. Phys.* **1970**, *9*, 553.
- (35) (a) We performed the detailed analyses of the interaction energies around the equilibrium structures by the energy decompositions using the symmetry-adapted perturbation theory (see Jeziorski, B.; Moszynski, R.; Szalewicz, K. *Chem. Rev.* **1994**, *94*, 1887. (b) The dispersion energies— E_{disp} are 4.12, 4.06, and 3.03 kcal/mol for $\text{C}_6\text{H}_6 \cdots \text{B}_2\text{H}_6$, $\text{C}_5\text{H}_6 \cdots \text{B}_2\text{H}_6$, and $\text{C}_4\text{H}_6 \cdots \text{B}_2\text{H}_6$, respectively. They are much larger than the electrostatic energies— E_{elst} : 2.68, 2.94, and 2.48 kcal/mol.
- (36) (a) Data are from the NIST webbook <http://webbook.nist.org/chemistry>. Cyclobutadiene: Kohn, D. W.; Chen, P. *J. Am. Chem. Soc.* **1993**, *115*, 2844. (b) 1,3-Cyclopentadiene: Kiselev, V. D.; Sakhabutdinov, A. G.; Shakirov, I. M.; Zverev, V. V.; Kononov, A. I. *Zh. Org. Khim.* **1992**, *228*, 2244. (c) Benzene: Nemeth, G. I.; Selzle, H. L.; Schlag, E. W. *Chem. Phys. Lett.* **1993**, *215*, 151.
- (37) Bent, H. A. *Chem. Rev.* **1961**, *61*, 275.